An Experimental Study of Multiphase Behavior for *n*-Butane/Bitumen/Water Mixtures

Jianyi Gao, University of Alberta; **Ryosuke Okuno,** University of Texas at Austin; and **Huazhou Andy Li,** University of Alberta

Summary

Steam/solvent coinjection has been studied and pilot tested as a potential method to improve steam-assisted gravity drainage (SAGD) for bitumen recovery. Reliable design of coinjection requires reliable pressure/volume/temperature (PVT) data for bitumen/solvent/water mixtures, which are scarce and fragmentary in the literature.

The main objective of this research was to present a new set of PVT and multiphase data for *n*-butane/Athabasca-bitumen/water mixtures at pressures up to 10 MPa and temperatures up to 160°C. Experiments were conducted with a conventional PVT apparatus. The data presented include multiphase equilibria up to four coexisting phases and liquid densities for 100% bitumen, two mixtures of *n*-butane/bitumen, and one mixture of *n*-butane/bitumen/water.

Liquid/liquid separation of hydrocarbons was experimentally observed at the *n*-butane concentration of 97 mol% in the *n*-butane/bitumen system with/without water, for a wide range of temperatures at operating pressures for expanding-solvent SAGD (ES-SAGD). This may indicate the limited solubility of *n*-butane in bitumen even when a high level of accumulation of *n*-butane takes place near a chamber edge in ES-SAGD for Athabasca bitumen. The multiphase transition that involves appearance/disappearance of the vapor phase was observed to occur near the vapor pressure of *n*-butane or its extension. Such phase transition occurs at a higher pressure in the presence of water, because of its vapor pressure, than in the absence of water at a given temperature. This is the first time four coexisting phases are reported for *n*-butane/Athabasca-bitumen/water mixtures at temperature/pressure conditions relevant to ES-SAGD.

Introduction

Steam injection has been widely implemented for heavy-oil/bitumen recovery (Prats 1982). SAGD is one of the most important applications of steam injection for bitumen recovery (Butler 1991). However, SAGD requires a substantial amount of water and energy resources for steam generation. The emission of carbon dioxide associated with steam generation is also a major environmental concern.

Coinjection of a small amount of solvent with steam, such as ES-SAGD, has been studied and pilot tested as a potential alternative to SAGD for bitumen recovery. Such coinjection processes aim to use thermal and compositional mechanisms to increase the mobility of the bitumen-rich phase near the chamber edge (e.g., Nasr and Isaacs 2001; Nasr et al. 2003). Various researchers showed that steam/solvent coinjection could result in incremental oil recovery compared with steam-only injection in laboratory-scale physical experiments, pole-scale experiments, and numerical simulations (e.g., Redford and McKay 1980; Li and Mamora 2010; Mohammadzadeh et al. 2012; Jha et al. 2012; Keshavarz et al. 2014). Ardali et al. (2012) concluded that solvent-assisted SAGD required lower energy and water consumption in comparison with SAGD.

This paper (SPE 180736) was accepted for presentation at the SPE Canada Heavy Oil Technical Conference, Calgary, 7–9 June 2016, and revised for publication. Original manuscript received for review 2 April 2016. Revised manuscript received for review 18 August 2016. Paper peer approved 8 September 2016.

Various hydrocarbons were tested as a potential coinjectant for steam/solvent coinjection. The choice of solvent at operating conditions depends on the composition of bitumen and PVT properties of phases. Redford and McKay (1980) indicated that injection of volatile components, such as propane and *n*-pentane, with steam into Athabasca bitumen resulted in a substantial in-situ retention of the solvents. Li et al. (2011) stated that heavy solvents, such as C_{12}, were the optimum solvents to be coinjected with steam for Athabasca bitumen. Yazdani et al. (2011) indicated that *n*-hexane and *n*-heptane were preferable for Athabasca bitumen in comparison with propane and *n*-pentane. Mohebati et al. (2010) found that steam–hexane coinjection could improve SAGD performance for Athabasca bitumen more than for that of Cold Lake and Lloydminster reservoirs.

Nasr et al. (2003) compared the drainage rates in coinjection of steam and solvents (methane to *n*-octane), and concluded that *n*-hexane and *n*-heptane were the optimum solvents for live Cold Lake bitumen. Mohebati et al. (2010) discussed that gaseous butane that accumulated near a chamber edge might limit the heat transfer to bitumen and reduce oil-drainage rate. Ardali et al. (2010) simulated the coinjection of steam and normal hydrocarbons (C_3 to C_7), and concluded that *n*-butane was the optimum solvent for Cold Lake with no initial solution gas at the operating pressure of 3400 kPa. Govind et al. (2008) observed a lower residual oil saturation simulated for *n*-butane coinjection at a higher operating pressure (4000 kPa).

Injection of solvent and steam into bitumen results in highly size-asymmetric polar mixtures, consisting of solvent, bitumen, and water. Design of solvent type and its concentration in coinjection requires a detailed understanding of multiphase behavior for solvent/bitumen/water mixtures at a wide range of temperatures at operating pressures (Nagarajan et al. 2006). There are many phase-behavior models for bitumen developed on the basis of experimental PVT data in the literature. Liquid/liquid boundaries and vapor/liquid/liquid boundaries for ternary mixtures of Athabasca bitumen, propane, and carbon dioxide were correlated by use of an advanced Peng-Robinson (PR) equation of state (EOS) (Díaz et al. 2011). This EOS was applied to predict phase boundaries and asphaltene precipitation in Agrawal et al. (2012), and was used for bitumen characterization on the basis of measured vapor pressures in Díaz et al. (2013). Kumar and Okuno (2016) developed a new algorithm for bitumen characterization by use of the PR EOS with the van der Waals mixing rules. The perturbed-chain form of the statistical association fluid theory (PC-SAFT) was also applied for bitumen characterization with the consideration of molecular association of asphaltene components (e.g., Panuganti et al. 2012; Leekumjorn and Krejbjerg 2013; Ma et al. 2016). PC-SAFT models have demonstrated good performance for modeling asphaltene precipitation (e.g., Tavakkoli et al. 2013; Zúñiga-Hinojosa et al. 2014). Zirrahi et al. (2015a, b) accurately predicted the solubility of carbon dioxide and water in bitumen by use of a cubic-plus association (CPA) EOS on the basis of the Soave-Redlich-Kwong (SRK) EOS and Wertheim's first-order thermodynamic perturbation theory for the association forces. Self- and cross-association parameters of bitumen components were adjusted to match experimental solubility data. A CPA EOS was also applied for predicting the solubility of light *n*-alkanes in

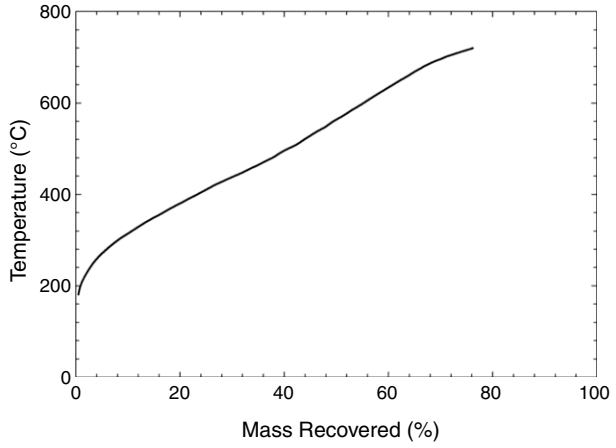

Fig. 1—Simulated distillation-test results of Athabasca-bitumen sample at temperature up to 720°C.

bitumen (Jindrová et al. 2015), and asphaltene precipitation (e.g., Li and Firoozabadi 2010; Jindrová et al. 2015). However, experimental phase-behavior data for solvent/bitumen/water mixtures are scarce and fragmentary in the literature.

Several papers reported experimental results for multiphase behavior associated with steam/solvent coinjection processes. Badamchi-Zadeh et al. (2009) measured saturation pressures and solubilities of propane in Athabasca bitumen at temperatures up to 50°C. Single liquid phase and liquid/vapor phase equilibria were visually observed with less than 20 wt% propane in bitumen/propane mixtures. A second dense phase was detected by in-line measurement of density and viscosity at propane concentrations above 20 wt% without visual confirmation. Kariznovi et al. (2011) developed a novel experimental design for phase-behavior studies, which was shown to be an effective method for phase detection and volume measurement. An in-line densitometer and a viscometer and gas chromatography (GC) were connected with an equilibrium cell to measure phase properties. They measured solubilities of propane in bitumen at temperatures from 50.9 to 149.8°C as well as phase densities and viscosities. Vapor/liquid equilibrium was detected at 100.5 and 149.8°C. Liquid/liquid equilibrium was detected at 50.9°C. Nourozieh et al. (2014) reported phase transitions for vapor/liquid and liquid/liquid equilibrium for *n*-butane/bitumen mixtures at temperatures up to 190°C. Agrawal et al. (2012) measured saturation pressures of a Peace River bitumen/*n*-pentane mixture (11 and 30 wt% *n*-pentane) from 90 to 180°C by use of a conventional PVT cell.

Amani et al. (2013) investigated the three-phase equilibrium for Athabasca bitumen/water mixtures, consisting of the vapor, aqueous, and bitumen-rich liquid phase. They measured phase boundaries for a series of mixtures with water concentrations from 9.2 to 89.7 wt% by use of an X-ray view cell. Amani et al. (2014) measured the three-phase behavior (water-rich, bitumen-rich, and vapor phases) for ternary mixtures of Athabasca bitumen, toluene, and water by use of X-ray transmission tomography. Water solubilities in the hydrocarbon-rich phase and density data of the water-saturated hydrocarbon phase were also presented. Volumetric properties for various bitumens and bitumen/solvent mixtures were also presented in the literature (e.g., Svrcek and Mehrotra 1982; Ashrafi et al. 2011; Saryazdi et al. 2013; Kariznovi et al. 2014; Nourozieh et al. 2014a, b, 2015a, b).

Glandt and Chapman (1995) stated that water-in-oil emulsion could appear near producing wells in SAGD. Water-in-oil emulsion and oil-in-water emulsion may exist in the wellhead effluent, but most of the studies about emulsion in SAGD were based on synthetic emulsion (e.g., Noik et al. 2005; Nguyen et al. 2013). Ezeuko et al. (2013) modeled in-situ formation of emulsification near a steam-chamber edge in SAGD and ES-SAGD (*n*-hexane, *n*-heptane, and *n*-octane solvents) by means of a two-stage pseudochemical reaction. They explained that a fraction of water might flow as water-in-oil emulsion in the oleic phase, which could improve the effective oil flow at the pore scale.

This paper presents an experimental study of multiphase behavior for *n*-butane/Athabasca-bitumen/water mixtures, which is part of a comprehensive study on the phase behavior of different solvents with Athabasca bitumen and water. The main objective in this paper is to study liquid/liquid separation of hydrocarbons when *n*-butane is mixed with Athabasca bitumen with/without water. The Experimental Section presents the experimental setup and procedure adopted in this research. The Results and Discussion section shows experimental results and gives an EOS model calibrated with the data. To our knowledge, this is the first time four coexisting phases are reported for *n*-butane/Athabasca-bitumen/water mixtures at temperature/pressure conditions relevant to ES-SAGD. A limited experimental observation is also reported for water-in-oil and oil-in-water emulsion observed during some of the experiments in this research.

Experimental Section

Materials. The molecular weight (MW) for the Athabasca bitumen was measured with a cryoscope (Cryette™, GAS 019-90, Precision Systems Inc., Natick, MA, USA) on the basis of freezing-point depression (Exova laboratory, Edmonton, Canada). The MW was measured to be 635 g/mol after preheating the sample to 60°C. The water content was measured to be 0.245 wt% and calculated to be 8.64 mol% in the bitumen sample (Exova laboratory, Edmonton, Canada), although the calculation is subject to various uncertainties, such as the bitumen MW. Removal of water from the bitumen sample by heating was not attempted, to prevent light components from being evaporated. The purity of the solvent used, which is *n*-butane (Praxair, Mississauga, Ontario, Canada), is 99.5%.

Saturates/aromatics/resins/asphaltenes analysis was conducted to obtain weight fractions of saturates, aromatics, resins, and asphaltenes in the bitumen sample by use of the liquid/solid chromatography method after preheating the sample to 60°C (Exova laboratory, Edmonton, Canada). The analysis indicated that the bitumen contains 28.6 wt% saturates, 30.7 wt% aromatics, 20.8 wt% Resins I, 1.8 wt% Resins II, and 18.0 wt% asphaltenes. Resins I were eluted from the column with methyl ethyl ketone. Resins II were then eluted from the column with tetrahydrofuran.

The compositional analysis was carried out with a high-temperature GC method, as described in ASTM D7169-05 (Exova laboratory, Edmonton, Canada) after preheating the sample to 60°C. The maximum boiling point reported was 720°C. The boiling-point distribution is shown in **Fig. 1** and **Table 1.** As presented in Díaz et al. (2011), boiling points above 30 wt% distilled for bitumen may be overestimated by simulated distillation.

Experimental Setup. Phase-behavior measurements for *n*-butane/Athabasca-bitumen and *n*-butane/Athabasca-bitumen/water mixtures were conducted with a conventional PVT apparatus (PVT-ZS-16-2-2-H/AC, DBR, Edmonton, Canada). **Fig. 2** shows a schematic for the apparatus. The operation limits of the PVT cell equipped in the PVT system are approximately 100 MPa (15,000 psi) and 199°C. The total sample capacity of the cell is 112 cm^3, and the height of the side window slot is 14.100 cm. An isolation piston with a thickness of 4.672 cm isolates the test fluid from hydraulic oil. The pressure of hydraulic oil is controlled by a high-pressure positive-displacement pump (PMP-500-1-20-HB, DBR, Edmonton, Canada). The temperature of the PVT cell is controlled by an air bath with a control accuracy of ±0.1°C. The PVT system is equipped with a cathetometer for direct volume measurement by measuring the height of the sample fluid or phases of interest. The uncertainty in volume measurement is ±0.016 cm^3. The accuracy of the Heise pressure gauge (901A-15K-232P-R5, Ashcroft Inc., Stratford, USA) assembled in the system is ±0.07% of full-scale 104 MPa (15,000 psig). A high-pressure precision-test gauge (700RG31, Fluke, Calgary, Canada) with an accuracy of ±0.01% of full-scale 69 MPa (10,000 psig) was also connected to the PVT cell for more-accurate pressure measurement. The dead volume of this PVT system is 1.754 cm^3.

Mass % Recovered	Temperature (°C)	Temperature (°F)	Mass % Recovered	Temperature (°C)	Temperature (°F)
0.5	181.0	357.8	39	489.3	912.7
1	203.4	398.1	40	495.9	924.6
2	226.4	439.5	41	501.6	934.9
3	244.3	471.7	42	506.8	944.2
4	258.6	497.5	43	513.7	956.7
5	270.3	518.5	44	521.4	970.5
6	280.7	537.3	45	528.6	983.5
7	290.3	554.5	46	535.8	996.4
8	299.2	570.6	47	542.2	1008.0
9	307.1	584.8	48	548.6	1019.5
10	314.2	597.6	49	556.8	1034.2
11	321.6	610.9	50	563.9	1047.0
12	328.9	624.0	51	570.2	1058.4
13	336.1	637.0	52	577.3	1071.1
14	343.0	649.4	53	584.7	1084.5
15	349.4	660.9	54	591.4	1096.5
16	355.4	671.7	55	598.4	1109.1
17	361.9	683.4	56	605.8	1122.4
18	368.4	695.1	57	613.1	1135.6
19	374.4	705.9	58	620.2	1148.4
20	380.3	716.5	59	627.1	1160.8
21	386.4	727.5	60	634.1	1173.4
22	392.4	738.3	61	640.9	1185.6
23	398.2	748.8	62	648.0	1198.4
24	404.3	759.7	63	654.4	1209.9
25	410.4	770.7	64	661.2	1222.2
26	416.6	781.9	65	668.4	1235.1
27	422.5	792.5	66	674.7	1246.5
28	427.7	801.9	67	681.2	1258.2
29	432.9	811.2	68	686.7	1268.1
30	438.0	820.4	69	692.0	1277.6
31	443.0	829.4	70	696.1	1285.0
32	448.1	838.6	71	701.1	1294.0
33	453.8	848.8	72	704.9	1300.8
34	459.3	858.7	73	708.7	1307.7
35	464.5	868.1	74	712.3	1314.1
36	470.4	878.7	75	715.8	1320.4
37	476.2	889.2	76	719.3	1326.7
38	481.9	899.4	76.2	720.0	1328.0

Table 1—Simulated distillation-test results of the bitumen sample.

A digital densitometer (DDM 2910, Rudolph Research Analytical, Hackettstown, New Jersey, USA) was used to measure liquid densities at atmospheric pressure. The accuracy of temperature control is ±0.05°C. The uncertainty of the density measurement by use of this densitometer is ±0.1 kg/m^3.

Experimental Procedure. Densities of the bitumen were measured with a digital densitometer (DDM 2910, Rudolph Research Analytical, Hackettstown, New Jersey, USA) at atmospheric pressure and temperature between 15.6 and 80.0°C. Densities of bitumen and *n*-butane/bitumen mixtures at reservoir conditions were

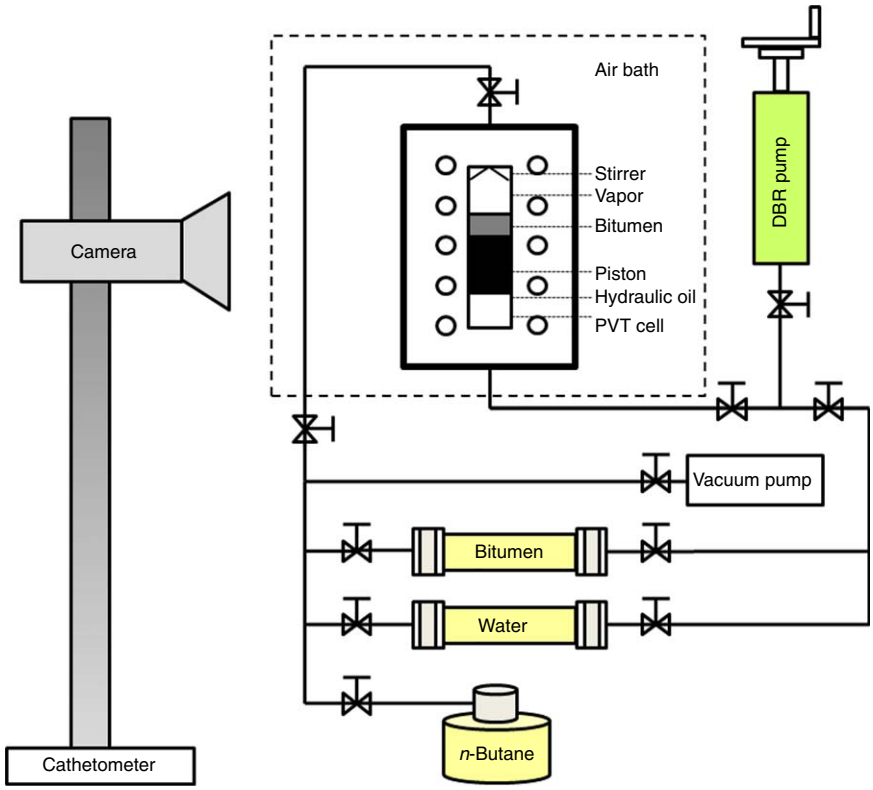

Fig. 2—Schematic of the experimental setup.

measured with the PVT cell on the basis of mass balance, as explained next. The density measurements were conducted at conditions of 15.6–160.0°C and 1.0–10.0 MPa.

Because the mass injected in the closed PVT cell was conserved, the density at a different temperature/pressure condition was obtained with the reference density that was measured at a known reference condition: that is,

$$\rho_2 = \frac{V_1}{V_2}\rho_1 = \frac{H_1}{H_2}\rho_1, \quad \ldots\ldots\ldots\ldots\ldots\ldots\ldots\ldots \quad (1)$$

where ρ_1, V_1, and H_1 are the sample's density (kg/m^3), volume (cm^3), and height in the PVT cell (cm) at the reference condition. ρ_2, V_2, and H_2 are the sample's density (kg/m^3), volume (cm^3), and height in the PVT cell (cm) at a given temperature/pressure condition. The reference density of bitumen was measured at 15.6°C and atmospheric pressure.

In this study, two *n*-butane/bitumen mixtures (Mixtures A and B) and one *n*-butane/bitumen/water mixture (Mixture C) were tested in the PVT equipment. The overall compositions of these mixtures are shown in **Table 2.** Multiphase equilibrium measurements were conducted with the constant composition expansion test method. Before each measurement, the PVT cell and inlet tubings were cleaned with toluene and evacuated by a vacuum pump. A sufficient amount of bitumen was stored in a transfer cylinder that was placed in the air bath of the PVT system. The high-pressure *n*-butane cylinder that was equipped with a dip tube allowed for direct withdrawal of liquid *n*-butane. It was directly connected to the inlet tubing of the PVT cell. After injecting a certain amount of liquid *n*-butane into the cell at room temperature, the air-bath temperature was set to 50.0°C for at least 12 hours, enabling the bitumen sample in the transfer cylinder and *n*-butane in the PVT cell to reach thermal equilibrium. The injected mass of liquid *n*-butane was calculated by use of the volume measured by the cathetometer and density values from the NIST database. The bitumen sample was then injected into the PVT cell without turning on the magnetic stirrer. After injection, the volume of bitumen was determined as the difference between the total volume and the liquid *n*-butane volume because no volume change upon mixing was assumed to occur for the short time period. The composition of this mixture was calculated on the basis of the densities, volumes, and MWs of bitumen and *n*-butane. After that, the temperature of the PVT cell was increased to the highest operating temperature in this research, 160.0°C. Subsequently, the mixture was vigorously stirred by the magnetic stirrer at 160.0°C for at least 12 hours to ensure that the components were completely mixed.

At each temperature, phase-boundary measurements were started from a single-liquid-phase state at a high pressure. Then, the pressure was gradually decreased by stepwise expansion at the rate of 3 cm^3/h. The mixture was sufficiently stirred for quickly reaching an equilibrium state before measurement at each pressure. Mixing by the stirrer was identified when circular movement for each fluid was observed inside the PVT cell. After reaching each specified pressure, the magnetic stirrer was switched off, and the system was kept static for a sufficient duration. An equilibrium state was deemed to be achieved when the cell pressure became

Mixture	Butane (mol%)	Bitumen (mol%)	Distilled Water (mol%)	Butane (wt%)	Bitumen (wt%)	Distilled Water (wt%)
A	72.23	27.77	0.00	19.19	80.81	0.00
B	97.24	2.76	0.00	76.29	23.71	0.00
C	37.02	1.05	61.93	54.65	16.97	28.37

Table 2—Compositions of three *n*-butane/bitumen/water mixtures in this research.

T (°C)	P (MPa)	ρ (kg/m^3)	T (°C)	P (MPa)	ρ (kg/m^3)
15.6	0.101	1010.4	50.1	4.100	992.1
20.0	0.101	1007.7	50.1	7.093	995.1
25.0	0.101	1004.4	50.1	10.106	997.9
30.0	0.101	1001.3	80.4	1.094	974.9
35.0	0.101	998.1	80.4	4.114	977.3
40.0	0.101	994.9	80.4	7.113	979.4
45.0	0.101	991.7	80.4	10.113	982.0
50.0	0.101	988.5	110.0	1.094	953.9
55.0	0.101	985.2	110.0	4.107	957.1
60.0	0.101	982.0	110.0	7.106	960.4
65.0	0.101	978.7	110.0	10.113	962.5
70.0	0.101	975.3	140.2	0.791	931.3
75.0	0.101	971.6	140.2	3.928	936.3
80.0	0.101	967.7	140.2	7.086	939.6
15.6	1.094	1012.7	140.2	10.119	942.7
15.6	4.107	1015.2	160.0	0.798	914.4
15.6	7.113	1016.6	160.0	3.831	922.1
15.6	10.113	1018.8	160.0	6.851	925.1
50.1	1.094	989.4	160.0	9.561	927.2

Table 3—Densities of bitumen at different temperature (T)/pressure (P) conditions. Measurement of density at 0.101 MPa was conducted by the densitometer. Densities of bitumen at pressures above 0.101 MPa were measured by use of a PVT cell.

steady. Two to three hours were sufficient for a single liquid phase to reach an equilibrium state at each temperature/pressure condition. The time allowed for equilibration was increased to four to five hours for multiphase equilibria. Thereafter, the phase-equilibrium state of the mixture was visually identified, and the volume of each phase was measured. For example, the phase interface between an *n*-butane-rich phase and a bitumen-rich phase was easily identified when the two phases showed distinct colors. It was observed that *n*-butane-rich liquid was colorless before mixing, but became dark red after mixing because *n*-butane extracted a significant amount of light and medium components from the bitumen. A phase-boundary pressure was first determined on the basis of visual observation of equilibrium phases, and then calculated by plotting the total volume (V) with respect to pressure (P). The PV relationship often showed a clear change in slope when a new phase appeared as pressure changed. Multiple phase boundaries for Mixtures A and B were sequentially determined with stepwise reduction of pressure at each temperature.

After completion of all measurements for Mixture B, a certain volume of distilled water was injected into the PVT cell to make the composition for Mixture C at approximately 50.0°C. The procedure described in the previous paragraph was applied to conduct phase-behavior tests for Mixture C starting at 160.0°C, the highest temperature in this research.

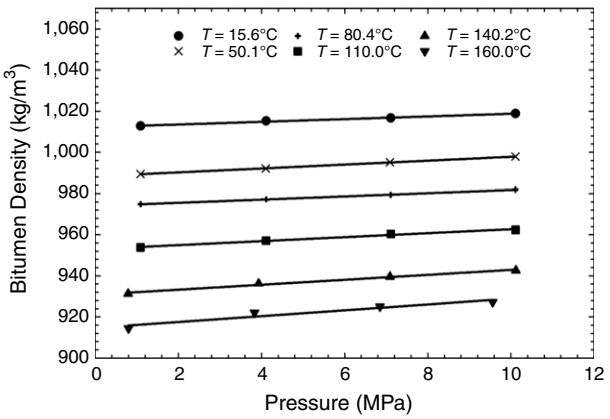

Fig. 3—Densities of bitumen measured with PVT cell at different temperatures. Solid lines are the trend lines matched with experimental data to illustrate the effect of temperature and pressure on bitumen density.

Results and Discussion

Bitumen. Table 3 gives bitumen densities measured at different temperatures and pressures. As expected, the density of bitumen decreased with increasing temperature at a constant pressure, and increased with increasing pressure at a constant temperature. In **Fig. 3,** the solid lines show that the effect of pressure on bitumen density is more significant at higher temperatures.

Measured densities were correlated with the Tait equation, taking into account the impact of pressure and temperature, as follows:

$$\rho(T,P)=\frac{\rho_0(T,P_0)}{1-\beta\ln\left(\frac{B+0.001P}{B+0.1}\right)}, \quad \ldots\ldots\ldots\ldots\ldots (2)$$

where

$$\rho_0 = 1149.3967 - 0.3822T - 3.5378\times10^{-4}T^2 \quad \ldots\ldots (3)$$

$$\beta = (-16.7695 + 0.0578T) \quad \ldots\ldots\ldots\ldots\ldots (4)$$

$$B = 3.7568\times10^4 - 1.8009\times10^7T^{-1} + 2.0605\times10^9T^{-2}. \quad \ldots\ldots\ldots\ldots\ldots (5)$$

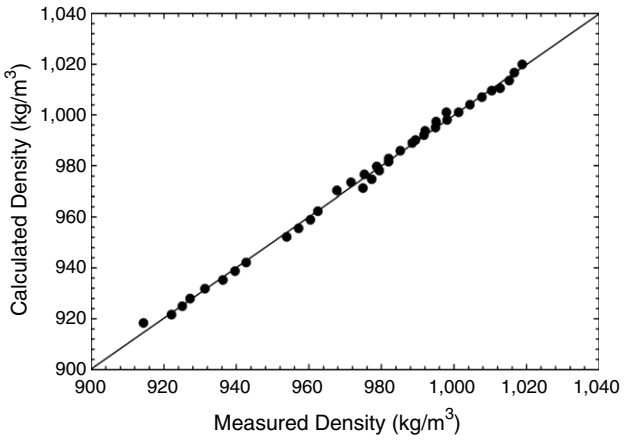

Fig. 4—The comparison between the calculated bitumen densities by use of the correlated Tait equation and experimental data.

In the previous equations, ρ is the density of bitumen in kg/m^3, ρ_0 is the density at atmospheric pressure, T is temperature in K, and P is pressure in kPa. **Fig. 4** indicates that the correlation yields a good match with experimental data. The coefficient of determination (R^2) for the correlated Tait equation is 0.9971, and the average absolute relative deviation (AARD) is 0.1%.

Saturation pressures of the bitumen sample were measured at 140.2°C and 160.0°C, as given in **Table 4.** The vapor phase was observed through the PVT-cell window. The total volume and volume of each phase were recorded with the cathetometer. For example, Appendix A shows the measured PV data for bitumen at 140.2°C, in which the saturation point can be clearly determined as the intersection of the two PV curves. **Table 5** shows the variation of liquid-phase and vapor-phase volume fractions measured at different pressures for the bitumen sample.

The bitumen was characterized by use of the PR EOS with the van der Waals mixing rules (Peng and Robinson 1976; Robinson and Peng 1978). For consistency, it was aimed to obtain a single set of parameters for the PR EOS to correlate all data obtained in this paper. The bitumen was split into four pseudo components (PCs) by use of the chi-squared distribution (Quiñones-Cisneros et al. 2004) with the degree of freedom of 4.0. The initial values of critical properties for PCs were calculated through the equations of Krejbjerg and Pedersen (2006). The binary interaction parameters (BIPs) between PCs were set to zero. The initial values of BIPs between water and PCs were calculated through the correlation presented in Venkatramani and Okuno (2016), as follows:

$$BIP = c_1[1+\exp(c_2 - c_3 MW)]^{-1/c_4}, \quad \ldots\ldots\ldots\ldots (6)$$

where $c_1 = 0.24200$, $c_2 = 65.90912$, $c_3 = 0.18959$, and $c_4 = -56.81257$. The BIPs between solvent and PCs were first calculated from the correlations used in Mehra (1981) and Li (1983) with the constant $n = 1$:

$$k_{ij} = 1 - \left(\frac{2\sqrt{V_{C_i}^{1/3} V_{C_j}^{1/3}}}{V_{C_i}^{1/3} + V_{C_j}^{1/3}}\right)^n, \quad \ldots\ldots\ldots\ldots\ldots\ldots (7)$$

where V_{C_i} and V_{C_j} are the critical volumes for components in cm^3/mol.

Then, stepwise adjustment on critical properties and BIPs was applied for matching all experimental data. Critical properties of PCs and BIPs for butane with PCs were adjusted to match L-LV boundaries for *n*-butane/bitumen (Mixture A), and LL-LLV boundaries for *n*-butane/bitumen (Mixture B). The water content, 8.64 mol%, in the bitumen sample yielded 2.4 mol% water in Mixture A and 0.2 mol% water in Mixture B. At this point, however, BIPs for water with PCs were not adjusted because of the low water contents in Mixtures A and B. Instead, water-PC BIPs were adjusted to match WLL-WLLV boundaries for Mixture C, in addition to the measured saturation pressures for the bitumen sample. Critical properties and BIPs were finalized primarily for accurate correlation of the phase-boundary data for the presence of the V phase. Then, volume-shift parameters (C_{PEN}) of PCs were used for matching liquid-density data. **Tables 6 and 7** present the components' parameters for use with the PR EOS, along with the overall compositions for all fluids discussed in this paper. In particular, it was challenging to represent multiphase-behavior data for the highly size-asymmetric polar mixtures of *n*-butane/bitumen/water, as will be shown in this paper.

The EOS model gives an AARD of 2.6% for the densities listed in Table 3. Table 4 compares the experimental data with the EOS predictions in terms of saturated-liquid density and saturation pressure. As given in this table, saturation-pressure data were accurately represented by the EOS model. The predicted densities at saturation pressures have the AARD of 6.0% compared with the experimental data. The predicted V phase composition from the EOS model is almost pure water, which is consistent with the measured-saturation pressures that are close to water-vapor pressures at corresponding temperatures. It is likely that the measured-saturation pressures (Table 4) are related to emulsified water in the bitumen sample.

Mixture A (72.23 mol% *n*-butane + 25.37 mol% bitumen + 2.40 mol% water). With the procedure mentioned in the Experimental Section, densities of Mixture A were measured at different temperature/pressure conditions, as summarized in **Table 8** and **Fig. 5.** The reference density was measured at 51.1°C and 1.115 MPa at AGAT laboratory, Calgary, Canada. Fig. 5 shows that the effect of pressure on density is more pronounced at higher temperatures for Mixture A.

Densities measured for Mixture A were first compared with the values calculated with the following equation assuming no volume change on mixing:

$$\frac{1}{\rho_m} = \frac{w_s}{\rho_s} + \frac{1-w_s}{\rho_B}, \quad \ldots\ldots\ldots\ldots\ldots\ldots\ldots\ldots (8)$$

where w_s is the weight fraction of *n*-butane. ρ_s and ρ_B are the mass densities of *n*-butane and bitumen, respectively. The values for ρ_s at different conditions were obtained from the NIST database. The ρ_B values were calculated from Eq. 2. The resulting AARD is 6.1%, which indicates that volume change on mixing should be taken into account for Mixture A.

An excess-volume mixing rule is given as

$$\frac{1}{\rho_m} = \frac{w_s}{\rho_s} + \frac{1-w_s}{\rho_B} - w_s(1-w_s)\left(\frac{1}{\rho_s} + \frac{1}{\rho_B}\right)\gamma, \quad \ldots\ldots\ldots (9)$$

	Experimental Data		Predictions From EOS Model	
T (°C)	P (MPa)	ρ^{sat} (kg/m^3)	P (MPa)	ρ^{sat} (kg/m^3)
140.2	0.337	932.8	0.349	983.6
160.0	0.484	917.9	0.436	978.4

Table 4—Measured and predicted saturation pressures and saturated-liquid densities of the bitumen sample. The vapor phase was only observed at 140.2 and 160.0°C in the saturation-pressure measurement for bitumen.

T (°C)	P (MPa)	Volume Fraction of Liquid Phase	Volume Fraction of Vapor Phase
140.2	0.322	0.933	0.067
140.2	0.322	0.887	0.113
140.2	0.315	0.852	0.148
140.2	0.301	0.820	0.180
140.2	0.301	0.791	0.209
140.2	0.288	0.752	0.248
160.0	0.481	0.960	0.041
160.0	0.467	0.858	0.142
160.0	0.467	0.761	0.240
160.0	0.322	0.933	0.067

Table 5—Measured liquid-phase and vapor-phase volume fractions of the bitumen sample at different temperature/pressure conditions.

where γ is the BIP between solvent (*n*-butane) and bitumen for this model. The best-fitted γ, 0.1548, was obtained by regression to the measured densities (Table 8). It gives the AARD of 1.3%, which is much lower than that from Eq. 8.

Saturation pressures were measured for Mixture A from 51.1 to 159.0°C. Single liquid phase and liquid/vapor phase equilibria were visually observed within this temperature range. The total volume and volume of each phase were recorded with the cathetometer. **Table 9** shows the variation of liquid-phase and vapor-phase volume fractions measured at different pressures for Mixture A. **Table 10** summarizes the results and the comparison with predictions from the EOS model (Tables 6 and 7). The EOS model reasonably correlates the measured bubblepoints as shown in **Fig. 6.** The AARD from the presented data is 46%. The aqueous (W) phase calculated by the EOS model (Fig. 6) was not observed experimentally, likely because of water-in-oil emulsion in the liquid (L) phase. Also, the calculated W phase is subject to the uncertainty associated with the water content measured for the bitumen sample. Although *n*-butane BIPs can be adjusted to obtain a higher correlative accuracy for a particular set of data, the EOS model has been developed by considering all experimental data obtained for all mixtures in this research, as mentioned

	MW	T_C (°C)	P_C (MPa)	ω	V_C (cm^3/mol)	C_{PEN} (cm^3/mol)	Bitumen (mol%)	Mixture A (mol%)	Mixture B (mol%)	Mixture C (mol%)
C_4	58.123	152.0	3.796	0.2014	254.617	–6.148	0.00	72.23	97.24	37.02
Water	18.010	373.9	22.064	0.3433	63.071	–0.091	8.64	2.40	0.24	62.02
PC–1	296.939	435.0	2.146	0.8423	612.873	–147.701	48.84	13.57	1.35	0.51
PC–2	662.802	495.1	1.507	0.9429	920.536	–275.005	21.88	6.08	0.60	0.23
PC–3	1082.668	725.0	1.364	1.0225	1,299.294	–447.976	13.40	3.72	0.37	0.14
PC–4	2003.494	1072.9	1.045	1.1486	2,192.365	–936.360	7.24	2.01	0.20	0.08

Table 6—Components' properties of the characterized EOS model and compositions for the fluids discussed in this research. Bitumen was characterized as a mixture of four pseudocomponents, PC-1, –2, –3, and –4. C_{PEN} is the volume-shift parameter of Péneloux et al. (1982).

	C_4	Water	PC–1	PC–2	PC–3
Water	0.6360				
PC–1	–0.0005	0.2006			
PC–2	–0.0011	0.1694	0.0000		
PC–3	–0.0018	0.1694	0.0000	0.0000	
PC–4	–0.0031	0.1694	0.0000	0.0000	0.0000

Table 7—Binary-interaction parameters used for the EOS model.

T (°C)	P (MPa)	ρ (kg/m^3)	T (°C)	P (MPa)	ρ (kg/m^3)
51.1	1.115	901.5	110.8	7.079	856.5
51.1	4.128	903.7	110.8	10.113	860.0
51.1	7.086	904.8	140.1	4.093	830.7
51.1	10.126	905.8	140.1	7.079	833.7
81.1	1.094	872.3	140.1	10.119	837.0
81.1	4.100	876.0	159.0	4.107	814.5
81.1	7.079	878.8	159.0	7.093	818.9
81.1	10.126	880.5	159.0	10.099	824.0
110.8	4.107	853.0			

Table 8—Densities of Mixture A measured at different temperature/pressure conditions by the PVT cell on the basis of constant-composition expansion.

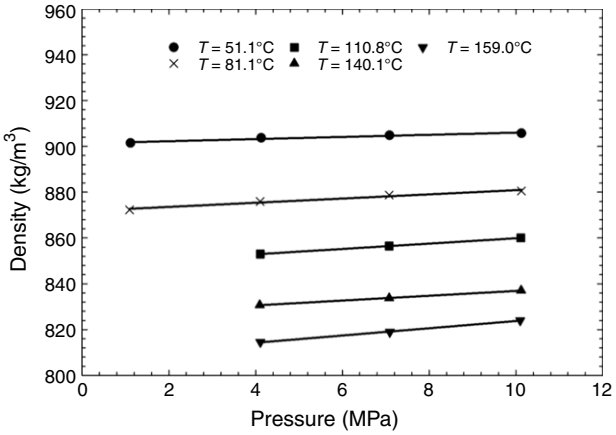

Fig. 5—Densities of Mixture A measured at a single liquid-phase state. Solid lines are the trend lines matched with experimental data.

previously. The predicted densities at saturation points by use of the EOS model give an AARD of 2.4% compared with experimental data (Table 10). For the data given in Table 8, the EOS model gives an AARD of 2.2%. The V phase composition predicted from the EOS model is almost pure butane.

Mixture B (97.24 mol% *n*-butane + 2.52 mol% bitumen + 0.24 mol% water). The mole fraction of *n*-butane in this mixture was specifically chosen for potentially observing three coexisting phases, consisting of the bitumen-rich liquid (L_1), solvent-rich liquid (L_2), and gaseous (V) phases. The phase-boundary pressures measured for Mixture B at different temperatures are listed in **Table 11.** These phase-boundary pressures were visually observed, and also confirmed by plotting pressure-volume (PV) data. For example, Appendix B shows the measured PV relationship at different temperatures. The slope for PV data exhibits a change when another phase emerges. Therefore, a phase-boundary pressure can be estimated by the intersection of PV segments. The volume of each phase was determined on the basis of visual observation of the interface between phases by use of the

T (°C)	*P* (MPa)	Volume Fraction of Liquid Phase	Volume Fraction of Vapor Phase
51.1	0.267	0.877	0.123
51.1	0.267	0.845	0.155
51.1	0.260	0.827	0.173
81.1	0.598	0.882	0.119
81.1	0.598	0.848	0.152
81.1	0.591	0.825	0.175
110.8	1.080	0.912	0.089
110.8	1.067	0.852	0.148
110.8	1.060	0.828	0.172
110.8	1.046	0.803	0.197
140.1	1.673	0.838	0.163
140.1	1.660	0.817	0.183
140.1	1.646	0.787	0.213
140.1	1.632	0.759	0.242
159.0	2.046	0.778	0.222
159.0	2.039	0.759	0.242
159.0	2.025	0.746	0.254

Table 9—Measured liquid-phase and vapor-phase volume fractions of Mixture A at different temperature/pressure conditions.

	Experimental Data		Predictions From EOS Model	
T (°C)	*P* (MPa)	ρ^{sat} (kg/m^3)	*P* (MPa)	ρ^{sat} (kg/m^3)
51.1	0.285	901.4	0.399	867.8
81.1	0.611	872.3	0.837	851.1
110.8	1.105	850.1	1.570	832.4
140.1	1.725	827.1	2.592	811.9
159.0	2.148	811.9	3.400	797.6

Table 10—Measured and predicted saturation pressures and densities at saturation points of Mixture A. One liquid phase equilibrium and liquid/vapor phase equilibrium were visually observed within this temperature range for Mixture A.

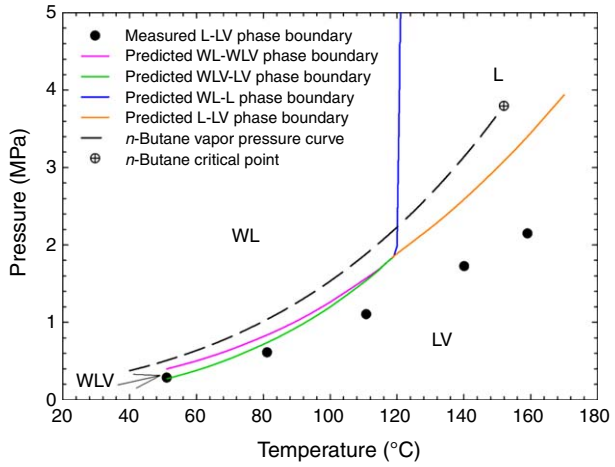

Fig. 6—Measured and predicted saturation pressures for Mixture A at different temperatures. The V phase is calculated to be almost pure butane.

cathetometer. The uncertainty in phase-boundary determination is affected by how clear the interface is. It is ± 0.791 MPa (100 psig) for measurement of L_2-L_1L_2 boundary and ± 0.174 MPa (10.5 psig) for L_1L_2-L_1L_2V boundary, except for the measurements at 50.0°C and 79.9°C. At these two temperatures, it was not

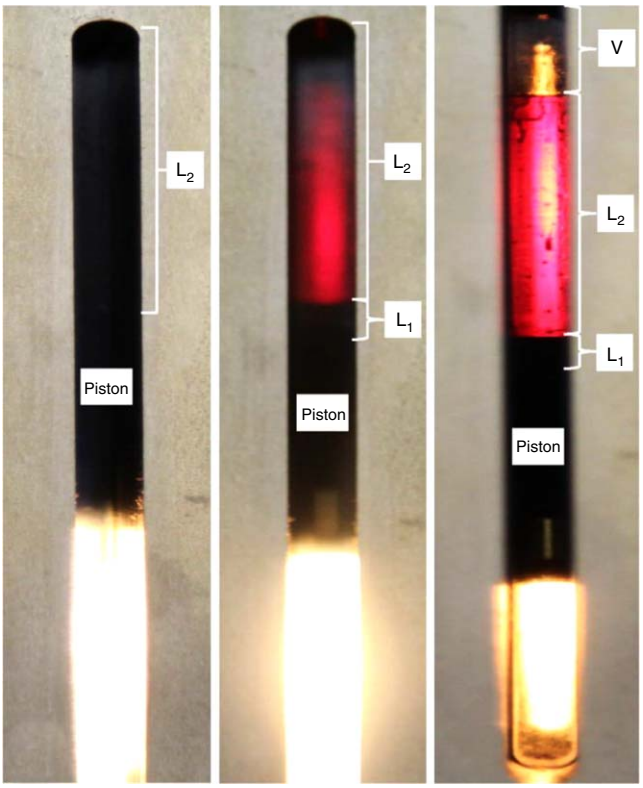

Fig. 7—Digital images of multiphase equilibrium captured for Mixture B: (a) Single liquid-phase equilibrium at 140.1°C and 11.105 MPa; (b) L_1L_2 equilibrium at 140.1°C and 8.375 MPa; and (c) L_1L_2V equilibrium at 140.1°C and 2.921 MPa. L_1 is bitumen-rich phase. L_2 is *n*-butane-rich phase. Phase boundaries were measured by stepwise pressure reduction and were based on visual observation of phases. The color of the L_2 phase became lighter with decreasing pressure, changing from black to red, indicating that *n*-butane extracted light and intermediate components more than heavier components from bitumen at lower pressures.

T (°C)	L_2-L_1L_2 (MPa)	L_1L_2-L_1L_2V (MPa)
50.0	1.679	0.517
79.9	2.735	0.983
109.8	4.380	1.761
140.1	9.118	2.946
160.2	16.633	4.033

Table 11—Measured phase-boundary pressures for Mixture B.

easy to determine the boundary between L_1 and L_2, likely because of their similarity in composition. Note that, because of the limited cell volume, the lower-pressure boundary for three phases could not be measured, and was not given in Table 11. Even when the piston was retracted to the limit of the PVT cell, the mixture still exhibited the three-phase equilibrium, as depicted by the asymptotic behavior of pressure depletion in Appendix B.

Fig. 7 shows the digital images of L_2, L_1L_2, and L_1L_2V phase equilibria captured at 140.1°C for Mixture B. At 140.1°C and 11.105 MPa, a single L_2 phase was detected; at this high pressure, liquid/liquid immiscibility did not take place. When the pressure was reduced to 8.375 MPa, liquid/liquid immiscibility appeared in the PVT cell (i.e., L_1L_2 equilibrium was observed). Both phases were not transparent. The L_1 phase was denser, black, and rich in bitumen, whereas the L_2 phase was less dense, red, and rich in *n*-butane. Because pure liquid *n*-butane is colorless, the red color of the L_2 phase implied that it selectively extracted a significant amount of intermediate components from the bitumen. The color of the L_2 phase became darker with increasing pressure and decreasing temperature, indicating more extraction of bitumen components. As the pressure was further decreased to 2.921 MPa, the V phase appeared, resulting in L_1L_2V equilibrium. Because of the limited cell volume, the L_1L_2V phases persisted even when the cell volume reached the maximum; therefore, the lower-pressure boundary of L_1L_2V was not detected. Compared with the L_2 phase at 8.375 MPa, the color of the L_2 phase was lighter at 2.921 MPa, implying that *n*-butane extracted a smaller amount of heavy components from the bitumen at L_1L_2V equilibrium, but still extracted light and medium components from the bitumen.

The L_1 phase in the L_1L_2 and L_1L_2V regions is considered to be richer in asphaltene components than the original bitumen because asphaltene components are insoluble in *n*-butane, as demonstrated in the research of Zou et al. (2007) for their bitumen/solvent mixtures. It is possible that asphaltene precipitation happened at the temperature/pressure conditions tested (even in the single L_2-phase region), considering the high *n*-butane concentration in the mixture. Asphaltene components may have resided in an oleic phase as dispersed particles, as described in Agrawal et al. (2012). However, it was not possible to observe asphaltene precipitation with the current PVT setup which is not equipped with a solid-phase detection unit.

Fig. 8 shows the comparison of experimental data and predictions for phase boundaries. The phase labeling in this figure is based on the continuity of phase compositions on phase transitions calculated from the EOS model. The three-phase region of L_1L_2V is predicted as a closed loop from the EOS model, near the higher-pressure boundary observed for three phases. However, the three phases observed at 50.0, 79.9, and 109.8°C are not represented by the EOS model. The lowest temperature for L_1L_2V equilibrium predicted from the EOS model is approximately 122.8°C. The AARD is 4.2% for the boundary for the presence of the V phase (i.e., bubblepoints), and 71% for the L-LL boundary from 140.1 to 160.2°C. Fig. 8 also shows that higher-pressure boundaries observed for three phases are well-correlated with the extension of *n*-butane's vapor pressure. EOS calculations further indicate that the L_1 and L_2 phases are close to each other near the critical temperature of *n*-butane in the LV two-phase region. This gives the dashed demarcation line between L_1V on the higher-temperature side and L_2V on the lower-temperature side

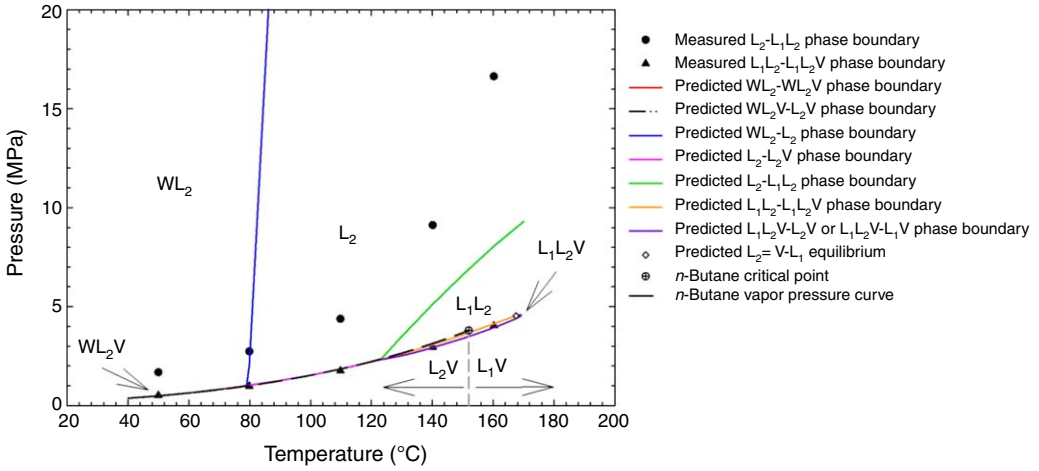

Fig. 8—Measured and predicted phase boundaries for Mixture B. The phase labeling in this figure is based on the continuity of phase compositions on phase transitions calculated from the EOS model. The three-phase region of L_1L_2V is predicted as a closed loop from the EOS model, near the higher-pressure boundary observed for three phases. However, the three-phase equilibriums observed at 50.0, 79.9, and 109.8°C are not represented by the EOS model. The lowest temperature for L_1L_2V predicted from the EOS model is approximately 122.8°C. Higher-pressure boundaries observed for three phases are well-correlated with the extension of *n*-butane's vapor pressure. EOS calculations further indicate that the L_1 and L_2 phases are close to each other near critical temperature of *n*-butane in the LV two-phase region. This gives the dashed demarcation line between L_1V on the higher-temperature side and L_2V on the lower-temperature side.

in Fig. 8. The W phase calculated by the EOS model was not experimentally observed for the same reasons mentioned in the previous section.

Results in this section indicate that *n*-butane was able to extract a significant amount of light and medium components from the bitumen in the L_2 phase, whereas the bitumen was substantially diluted by *n*-butane in the L_1 phase. The total weight fraction of lighter bitumen PCs (PC-1 and PC-2) in the L_2 phase is calculated to be approximately 11 wt% (2.0 mol%) in the L_1L_2 equilibrium region at 140.1°C, and approximately 24 wt% (6.1 mol%) in the three-phase region by use of the PR-EOS model. The L_1 phase is calculated to contain approximately 81 wt% (17 mol%) bitumen components in the L_1L_2 equilibrium region, and 64 wt% (12 mol%) bitumen components in the L_1L_2V region. The L_1 and L_2 phases may contribute to the overall production of bitumen in ES-SAGD. However, the effect of the resulting multiphase flow on bitumen production is uncertain. The solubility of butane in bitumen may be limited by the L_1L_2 separation at operating conditions for steam/solvent coinjection, such as ES-SAGD, even when a sufficient accumulation of *n*-butane takes place near a chamber edge. Experimental observations given in Fig. 8 show that the L_1L_2 separation may occur at a wide range of temperatures at operating pressures in ES-SAGD.

Mixture C (37.02 mol% *n*-butane + 0.96 mol% bitumen + 62.02 mol% water). After the multiphase equilibrium measurements for Mixture B, 7.389 g of distilled water was injected into the PVT cell. Four coexisting phases, consisting of L_1, L_2, V, and W phases, were observed over a wide range of temperature/pressure conditions. **Table 12** summarizes the phase-boundary pressures measured for Mixture C at different temperatures. The phase-boundary measurement was also attempted at 50.0°C. However, it was difficult because of water-in-oil and oil-in-water emulsion formation, as briefly discussed in the next subsection.

T (°C)	WL_2-WL_1L_2 (MPa)	WL_1L_2-WL_1L_2V (MPa)
80.0	6.633	1.071
110.0	8.050	1.955
140.0	9.411	3.439
159.9	11.820	4.807

Table 12—Measured phase-boundary pressures for Mixture C.

Appendix C shows the measured PV data for Mixture C at different temperatures. Phase-boundary pressures were confirmed by visual observation and by the intersections of PV segments for each temperature. The uncertainty in measurement is ± 1.136 MPa (150 psig) for WL_2-WL_1L_2 phase boundaries and ± 0.174 MPa (10.5 psig) for WL_1L_2-WL_1L_2V boundaries, except for the measurements at 80.0°C and 110°C. At these two temperatures, the interface between the L_1 and L_2 phases was unclear from visual observation and PV plots (Appendix C).

Fig. 9 shows the digital photos taken during the phase-equilibrium tests for Mixture C. At the temperature/pressure conditions in this research, the W phase was always denser than the L_1 phase. As can be seen in Fig. 9, the W phase was transparent, but contained some hydrocarbon droplets that were denser than the water; that is, the droplets likely consisted of bitumen components, e.g., asphaltenes. At 159.9°C and 27.687 MPa, the W and L_2 phases were observed, where the W phase was below the L_2 phase. When the pressure declined to 8.258 MPa, liquid/liquid separation of hydrocarbons happened, resulting in the WL_1L_2 equilibrium. In this WL_1L_2 equilibrium, the L_1 phase was between the W and L_2 phases. The L_2 phase showed a lighter color than the L_1 phase because of a higher fraction of *n*-butane. With the pressure further decreasing to 4.576 MPa, the four-phase equilibrium of WL_1L_2V was detected, where the V phase appeared on top of the existing phases. The L_2 phase became lighter color than at 8.258 MPa, implying that *n*-butane extracted a smaller amount of heavy components from the bitumen at WL_1L_2V equilibrium. Again, because of the limited PVT cell volume, the WL_1L_2V phase equilibria persisted all the way up to the maximum cell volume, and the lower phase boundary was not detected.

Fig. 10 compares the phase boundaries observed with those from the EOS model (Tables 6 and 7) for Mixture C. The phase labeling in this figure is based on the EOS model as for Fig. 8. The AARD is 1.1% for the boundary for the presence of the vapor phase, and 33% for the WL-WLL boundary at temperatures from 140.0°C to 159.9°C. The higher-pressure boundaries for the four phases are calculated close to the extension of *n*-butane's vapor pressure; however, they are higher than the corresponding vapor pressures of *n*-butane, unlike in Mixture B (Fig. 8). This is likely because the higher-pressure boundary for the presence of the V

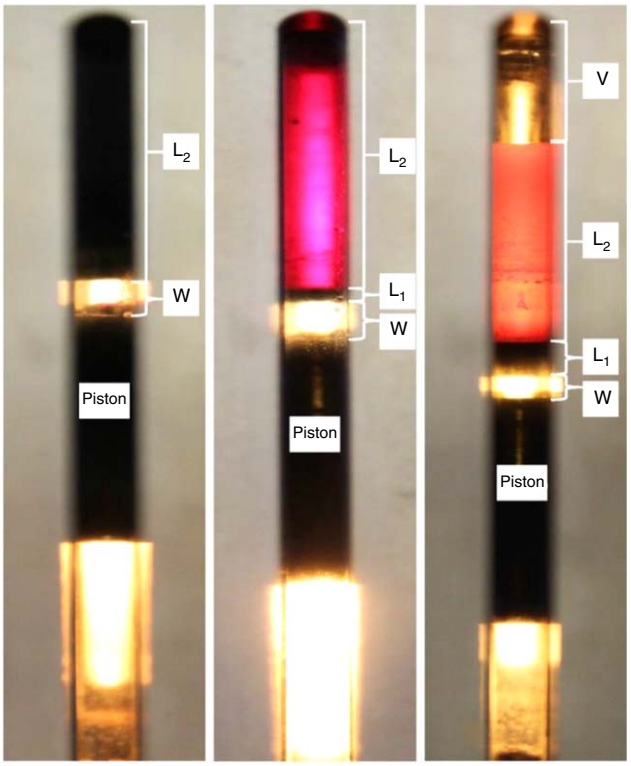

Fig. 9—Digital images of multiphase equilibrium captured for Mixture C: (a) WL_2 equilibrium at 159.9°C and 27.687 MPa; (b) WL_1L_2 equilibrium at 159.9°C and 8.258 MPa; and (c) WL_1L_2V equilibrium at 159.9°C and 4.576 MPa. L_1 is bitumen-rich phase. L_2 is *n*-butane-rich phase. The W phase was denser than the L_1 phase at the temperature/pressure conditions in this research.

phase for Mixture C (Fig. 10) is increased by water-vapor pressure, compared with that for Mixture B (Fig. 8). The four-phase region of WL_1L_2V is predicted as a closed loop from the EOS model, near the lower-pressure boundaries measured for the WL_1L_2 region. As mentioned previously, however, no lower-pressure boundary for WL_1L_2V was observed experimentally. The phase transition between three and four phases was not represented by the EOS model at 80.0 and 110.0°C. The EOS model gives a large deviation in representing the WL_2-WL_1L_2 boundary at lower temperatures. As mentioned previously, the interface between L_1 and L_2 tended to be unclear at lower temperatures. The phase compositions of L_1 and L_2 are calculated to be close to each other near the critical temperature of *n*-butane in the WLV region (either WL_1V or WL_2V in Fig. 10).

Oil-in-Water and Water-in-Oil Emulsion. The series of isothermal experiments for Mixture C were conducted from the highest temperature, 159.9°C, and then the temperature was decreased in a stepwise manner. It became more difficult to observe the W phase at lower temperatures mainly because of oil-in-water emulsion caused by the repeated usage of the PVT-cell stirrer.

After the multiphase equilibrium measurements for Mixture B, distilled water was injected into the PVT cell at 50.0°C and 5.617 MPa (800 psig). Without turning on the magnetic stirrer before measurements for Mixture C, W-L_2 phases were clearly observed in the PVT cell at this temperature/pressure condition. After a series of measurements from 159.9°C to 50.0°C, however, there was only one single liquid phase in the PVT cell at the same temperature/pressure condition, 50.0°C and 5.617 MPa.

Then, the pressure was reduced to 0.1 MPa at 50.0°C, and water was observed, as shown in **Fig. 11.** Fig. 11b is an enlarged photo for the detected water. The existence of oil-in-water emulsion can be also confirmed by the comparison with the clear W phase at 159.9°C given in Fig. 9. The overall composition is identical in these two figures.

Also, water-in-oil emulsion likely occurred because water came out of the hydrocarbon liquid phases as water-in-oil emulsion, instead of as a separate bulk phase, as the temperature was decreased. This type of water precipitation in the oleic phase was described also in Glandt and Chapman (1995). In this research, water-in-oil emulsion was confirmed by comparing the mass of injected water (7.389 g) and the mass of the W phase after completing measurements (7.347 g).

Conclusions

This paper presented an experimental study of multiphase behavior for *n*-butane/Athabasca-bitumen/water mixtures at

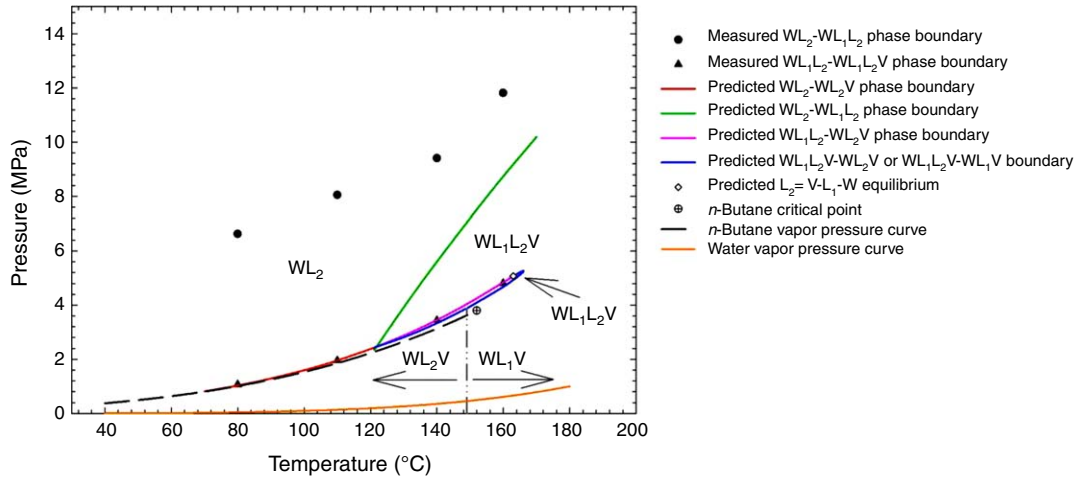

Fig. 10—Measured and predicted phase boundaries for Mixture C. The phase labeling in this figure is based on the EOS model. The higher-pressure boundaries for the four phases are observed close to the extension of *n*-butane's vapor pressure; however, they are higher than the corresponding vapor pressures of *n*-butane, unlike in Mixture B (Fig. 8). The four-phase region of WL_1L_2V is predicted as a closed loop from the EOS model, near the lower-pressure boundaries measured for the WL_1L_2 region. However, no lower-pressure boundary for WL_1L_2V was observed experimentally. The phase transition between three and four phases was not represented by the EOS model at 80.0 and 110.0°C. The EOS model gives a large deviation for the WL_2-WL_1L_2 boundary at lower temperatures; as mentioned previously, the interface between L_1 and L_2 was not clear at lower temperatures. The phase compositions of L_1 and L_2 are calculated to be close to each other near *n*-butane's critical temperature in the WLV region (WL_1V or WL_2V).

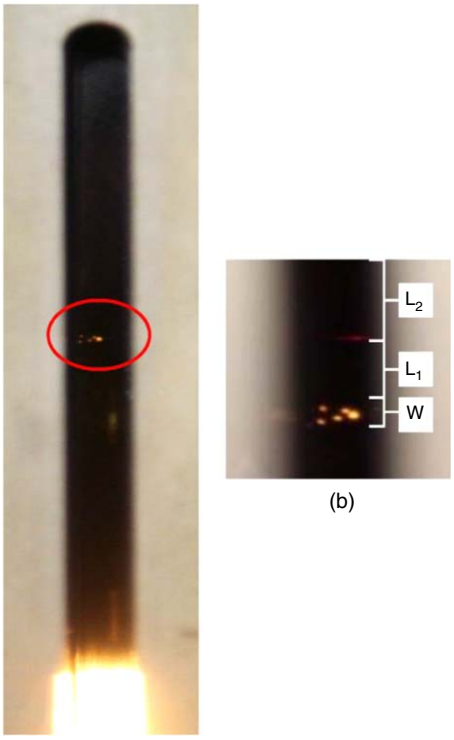

Fig. 11—(a) Water phase is not transparent because of oil-in-water emulsion at 50.0°C for Mixture C. Shining points indicate the presence of water. (b) Enlarged photo of detected water in the PVT cell.

temperatures up to 160°C and pressures up to 10 MPa. The data presented in this paper include liquid densities and multiphase boundaries for 100% bitumen, two mixtures of *n*-butane/bitumen, and one mixture of *n*-butane/bitumen/water. Although limited in correlative accuracy, a single thermodynamic model was made to correlate all data measured for all mixtures on the basis of the PR EOS with the van der Waals mixing rules. Conclusions are as follows:

- Liquid/liquid separation of hydrocarbons (L_1L_2) was experimentally observed at the butane concentration of 97 mol% in the *n*-butane/bitumen system with/without water (Mixtures B and C) for a wide range of temperatures at operating pressures for ES-SAGD. This may indicate the limited solubility of butane in bitumen even when a high level of accumulation of butane takes place near a chamber edge in ES-SAGD for Athabasca bitumen.
- It was observed that the color of the L_2 phase became lighter with decreasing pressure in the LLV region for Mixture B and in the WLLV region for Mixture C. This may indicate the selective extraction of bitumen components by *n*-butane at lower pressure; the L_2 phase became richer in lighter PCs rapidly with decreasing pressure in the LLV region for Mixture B and in the WLLV region for Mixture C.
- The multiphase transition that involves appearance/disappearance of the V phase was observed to occur near the vapor pressure of *n*-butane or its extension. Such phase transition occurs at a higher pressure in the presence of water (Mixture C), because of its vapor pressure, than in the absence of water (Mixture B) at a given temperature.
- Water-in-oil emulsion may occur when dissolved water in the oleic phase comes out of the solution at a lower temperature even without significant stirring.
- Near-miscibility of two liquid phases and oil-in-water emulsion made it difficult to conduct phase-boundary measurements in this research. The experimental setup and/or procedure should be improved in this regard.

Nomenclature

C_{PEN} = Peneloux volume-shift parameter
P_c = critical pressure
T_c = critical temperature
V_c = critical volume
ω = acentric factor

Acknowledgments

Research grants from Japan Petroleum Exploration Co. Ltd. and Japan Canada Oil Sands Ltd. through the Center for Petroleum and Geosystems Engineering at the University of Texas at Austin and the Natural Sciences and Engineering Research Council of Canada (RGPIN 418266 and RGPIN 05394) are greatly acknowledged. We thank Francisco Javier Argüelles Vivas for technical suggestions for the experiments. We also thank the laboratory technician, Todd Kinnee, for his assistance in the PVT experiments at the University of Alberta. Ryosuke Okuno holds the Pioneer Corporation Faculty Fellowship in Petroleum Engineering at the University of Texas at Austin.

References

Agrawal, P., Schoeggl, F. F., Satyro, M. A. et al. 2012. Measurement and Modeling of the Phase Behavior of Solvent Diluted Bitumens. *Fluid Phase Equilibria* **334:** 51–64. https://doi.org/10.1016/j.fluid.2012.07.025.

Amani, M. J., Gray, M. R., and Shaw, J. M. 2013. Phase Behavior of Athabasca Bitumen + Water Mixtures at High Temperature and Pressure. *J. Supercri. Fluid* **77:** 142–152. https://doi.org/10.1016/j.supflu.2013.03.007.

Amani, M. J., Gray, M. R., and Shaw, J. M. 2014. The Phase Behavior of Athabasca Bitumen+Toluene+Water Ternary Mixtures. *Fluid Phase Equilibr.* **370:** 75–84. https://doi.org/10.1016/j.fluid.2014.02.028.

Ardali, M., Mamora, D. D., and Barrufet, M. 2010. A Comparative Simulation Study of Addition of Solvents to Steam in SAGD Process. Presented at the Canadian Unconventional Resources and International Petroleum Conference, Calgary, 19–21 October. SPE-138170-MS. https://doi.org/10.2118/138170-MS.

Ardali, M., Barrufet, M., and Mamora, D. D. 2012. Laboratory Testing of Addition of Solvents to Steam to Improve SAGD Process. Presented at the SPE Heavy Oil Conference Canada, Calgary, 12–14 June. SPE-146993-MS. https://doi.org/10.2118/146993-MS.

Arshad, M. and Li, H. 2015. Multiphase Equilibria of Solvent-Steam-Bitumen System Within SAGD Steam-Chamber Boundary. Presented at the SPE Heavy Oil Conference-Canada, Calgary, 11–13 June. SPE-174444-MS. https://doi.org/10.2118/174444-MS.

Ashrafi, M., Souraki, Y., Karimaie, H. et al. 2011. Experimental PVT Property Analyses for Athabasca Bitumen. Presented at the Canadian Unconventional Resources Conference, Calgary, 15–17 November. SPE-147064-MS. https://doi.org/10.2118/147064-MS.

Badamchi-Zadeh, A., Yarranton, H. W., Svrcek, W. Y. et al. 2009. Phase Behaviour and Physical Property Measurements for VAPEX Solvents: Part I. Propane and Athabasca bitumen. *J Can Pet Technol* **48** (1): 54–61. PETSOC-09-01-54. https://doi.org/10.2118/09-01-54.

Butler, R. M. 1991. *Thermal Recovery of Oil and Bitumen.* New Jersey: Prentice Hall.

Díaz, O. C., Modaresghazani, J., Satyro, M. A. et al. 2011. Modeling the Phase Behavior of Heavy Oil and Solvent Mixtures. *Fluid Phase Equilibr.* **304** (1): 74–85. https://doi.org/10.1016/j.fluid.2011.02.011.

Díaz, O. C., Schoeggl, F. F., Yarranton, H. W. et al. 2013. Measurement of Heavy Oil and Bitumen Vapor Pressure for Fluid Characterization. *Ind. & Eng. Chem. Res.* **52** (8): 3027–3035. https://doi.org/10.1021/ie303397y.

Ezeuko, C. C., Wang, J., and Gates, I. D. 2013. Investigation of Emulsion Flow in Steam-Assisted Gravity Drainage. *SPE J.* **18** (3): 440–447. SPE-157830-PA. https://doi.org/10.2118/157830-PA.

Glandt, C. A. and Chapman, W. G. 1995. The Effect of Water Dissolution on Oil Viscosity. *SPE Res Eng* **10** (1): 59–64. SPE-24631-PA. https://doi.org/10.2118/24631-PA.

Govind, P. A., Das, S. K., Srinivasan, S. et al. 2008. Expanding Solvent SAGD in Heavy Oil Reservoirs. Presented at the 2008 SPE International Thermal Operations and Heavy Oil Symposium, Calgary, 20–23 October. SPE-117571-MS. https://doi.org/10.2118/117571-MS.

Jha, R. K., Kumar, M., Benson, I. et al. 2012. New Insights Into Steam-Solvent Co-injection Process Mechanism. Presented at the 2012 SPE Annual Technical Conference and Exhibition, San Antonio, Texas, 8–10 October. SPE-159277-MS. https://doi.org/10.2118/159277-MS.

Jindrová, T., Mikyška, J., and Firoozabadi, A. 2015. Phase Behavior Modeling of Bitumen and Light Normal Alkanes and CO_2 by PR-EOS and CPA-EOS. *Energy Fuels* **30** (1): 515–525. https://doi.org/10.1021/acs.energyfuels.5b02322.

Kariznovi, M., Nourozieh, H., and Abedi, J. 2011. Experimental Apparatus for Phase Behavior Study of Solvent–Bitumen Systems: A Critical Review and Design of a New Apparatus. *Fuel* **90** (2): 536–546. https://doi.org/10.1016/j.fuel.2010.10.019.

Kariznovi, M., Nourozieh, H., and Abedi, J. 2014. Measurement and Correlation of Viscosity and Density for Compressed Athabasca Bitumen at Temperatures Up to 200°C. *J Can Pet Technol* **53** (6): 330–338. SPE-173182-PA. https://doi.org/10.2118/173182-PA.

Keshavarz, M., Okuno, R., and Babadagli, T. 2014. Efficient Oil Displacement Near the Chamber Edge in ES-SAGD. *J. Petro. Sci. Eng.* **118:** 99–113. https://doi.org/10.1016/j.petrol.2014.04.007.

Krejbjerg, K. and Pedersen, K. S. 2006. Controlling VLLE Equilibrium With a Cubic EOS in Heavy Oil Modeling. Presented at the Canadian International Petroleum Conference, Calgary, 13–15 June. PETSOC-2006-052. https://doi.org/10.2118/2006-052.

Kumar, A. and Okuno, R. 2016. A New Algorithm for Multiphase Fluid Characterization for Solvent Injection. Accepted for publication in *SPE J*. on March 8, 2016. SPE-175123-PA. https://doi.org/dx.doi.org/10.2118/175123-PA.

Leekumjorn, S. and Krejbjerg, K. 2013. Phase Behavior of Reservoir Fluids: Comparisons of PC-SAFT and Cubic EOS Simulations. *Fluid Phase Equilibr.* **359:** 17–23. https://doi.org/10.1016/j.fluid.2013.07.007.

Li, Y. K. 1983. Heavy Fraction Characterization and Hypothetical Component Selection for Oil and Gas Mixtures. Computer Modelling Group Research Report R12.04. May 1983.

Li, W. and Mamora, D. D. 2010. Phase Behavior of Steam With Solvent Co-injection Under Steam Assisted Gravity Drainage (SAGD) Process. Presented at the SPE EUROPEC/EAGE Annual Conference and Exhibition, Barcelona, 14–17 June. SPE-130807-MS. https://doi.org/10.2118/130807-MS.

Li, Z. and Firoozabadi, A. 2010. Modeling Asphaltene Precipitation by *n*-Alkanes From Heavy Oils and Bitumens Using Cubic-Plus-Association Equation of State. *Energy and Fuels* **24** (2): 1106–1113. https://doi.org/10.1021/ef9009857.

Li, W., Mamora, D. D., and Li, Y. 2011. Solvent-Type and Ratio Impacts on Solvent-Aided SAGD Process. *SPE Res. Eval. & Eng.* **14** (3): 320–331. SPE-130802-PA. https://doi.org/10.2118/130802-PA.

Ma, M., Chen, S., and Abedi, J. 2016. Predicting the Multiphase Equilibrium and Density of Bitumen With C2H6, C3H8 and CO_2 Using the Simplified PC-SAFT Equation of State. *Fuel* **181:** 652–659. https://doi.org/10.1016/j.fuel.2016.05.040.

Mehra, R. K. 1981. *The Computation of Multi-Phase Equilibrium in Compositional Reservoir Studies*. PhD dissertation, University of Calgary.

Mohammadzadeh, O., Rezaei, N., and Chatzis, I. 2012. More Insight Into the Pore-Level Physics of the Solvent-Aided SAGD (SA-SAGD) Process for Heavy Oil and Bitumen Recovery. Presented at the SPE Heavy Oil Conference Canada, Calgary, 12–14 June. SPE-157776-MS. https://doi.org/10.2118/157776-MS.

Mohebati, M. H., Maini, B. B., and Harding, T. G. 2010. Optimization of Hydrocarbon Additives With Steam in SAGD for Three Major Canadian Oil Sands Deposits. Presented at the Canadian Unconventional Resources and International Petroleum Conference, Calgary, 19–21 October. SPE-138151-MS. https://doi.org/10.2118/138151-MS.

Nagarajan, N. R., Honarpour, M. M., and Sampath, K. 2006. Reservoir Fluid Sampling and Characterization—Key to Efficient Reservoir Management. Presented at the Abu Dhabi International Petroleum Exhibition and Conference, Abu Dhabi, 5–8 November. SPE-101517-MS. https://doi.org/10.2118/101517-MS.

Nasr, T. N. and Isaacs, E. 2001. Process for Enhancing Hydrocarbon Mobility Using a Steam Additive. US Patent 6230814.

Nasr, T. N., Beaulieu, G., Golbeck, H. et al. 2003. Novel Expanding Solvent-SAGD Process "ES-SAGD". *J Can Pet Technol* **42** (1): 13–16. PETSOC-03-01-TN. https://doi.org/10.2118/03-01-TN.

Nguyen, D., Phan, J., and Balsamo, V. 2013. Effect of Diluents on Interfacial Properties and SAGD Emulsion Stability: I. Interfacial Rheology. Presented at the SPE Heavy Oil Conference Canada, Calgary, 11–13 June. SPE-165405-MS. https://doi.org/10.2118/165405-MS.

Noik, C., Dalmazzone, C. S., Goulay, C. et al. 2005. Characterisation and Emulsion Behaviour of Athabasca Extra Heavy Oil Produced by SAGD. Presented at the 2005 SPE International Thermal Operations and Heavy Oil Symposium, Calgary, 1–3 November. SPE-97748-MS. https://doi.org/10.2118/97748-MS.

Nourozieh, H., Kariznovi, M., and Abedi, J. 2014a. Measurement and Prediction of Density for the Mixture of Athabasca Bitumen and Pentane at Temperatures up to 200°C. *Energy Fuels* **28** (5): 2874–2885. https://doi.org/10.1021/ef4022784.

Nourozieh, H., Kariznovi, M., and Abedi, J. 2014b. Phase Behaviour Study of Butane/Athabasca Bitumen Mixtures Applicable for Thermal and Hybrid Solvent Recovery Processes. Presented at the SPE Heavy Oil Conference-Canada, Calgary, 10–12 June. SPE-170163-MS. https://doi.org/10.2118/170163-MS.

Nourozieh, H., Kariznovi, M., and Abedi, J. 2015a. Modeling and Measurement of Thermo-Physical Properties for Athabasca Bitumen and *n*-Heptane Mixtures. *Fuel* **157:** 73–81. https://doi.org/10.1016/j.fuel.2015.04.032.

Nourozieh, H., Kariznovi, M., and Abedi, J. 2015b. Measurement and Prediction of Volumetric Properties for Undersaturated Athabasca Bitumen. *Energy Fuels* **29** (8): 4711–4720. https://doi.org/10.1021/acs.energyfuels.5b00128.

Nourozieh, H., Kariznovi, M., and Abedi, J. 2015c. Experimental and Modeling Studies of Phase Behavior for Propane/Athabasca Bitumen Mixtures. *Fluid Phase Equilibr.* **397:** 37–43. https://doi.org/10.1016/j.fluid.2015.03.047.

Nourozieh, H., Kariznovi, M., and Abedi, J. 2015d. Density and Viscosity of Athabasca Bitumen Samples at Temperatures Up to 200°C and Pressures Up to 10 MPa. *SPE Res Eval & Eng* **18** (3): 375–386. SPE-176026-PA. https://doi.org/10.2118/176026-PA.

Panuganti, S. R., Vargas, F. M., Gonzalez, D. L. et al. 2012. PC-SAFT Characterization of Crude Oils and Modeling of Asphaltene Phase Behavior. *Fuel* **93:** 658–669. https://doi.org/10.1016.j.fuel.2011.09.028.

Péneloux, A., Rauzy, E., and Fréze, R. 1982. A Consistent Correction for Redlich-Kwong-Soave Volumes. *Fluid Phase Equilibr.* **8** (1): 7–23. https://doi.org/10.1016/0378-3812(82)80002-2.

Peng, D. Y. and Robinson, D. B. 1976. A New Two-constant Equation of State. *Ind. Eng. Chem. Fund.* **15** (1): 59–64. https://doi.org/10.1021/i160057a011.

Prats, M. 1982. *Thermal Recovery*. SPE Monograph Series, Vol. 7, Henry L. Doherty Series, New York.

Quiñones-Cisneros, S. E., Dalberg, A., and Stenby, E. H. 2004. PVT Characterization and Viscosity Modeling and Prediction of Crude Oils. *Petro. Sci. Tech.* **22** (9–10): 1309–1325. https://doi.org/10.1081/LFT-200034092.

Redford, D. A. and McKay, A. S. 1980. Hydrocarbon-Steam Processes for Recovery of Bitumen From Oil Sands. Presented at the SPE/DOE Enhanced Oil Recovery Symposium, Tulsa, 20–23 April. SPE-8823-MS. https://doi.org/10.2118/8823-MS.

Robinson, D. B. and Peng, D. Y. 1978. The Characterization of the Heptanes and Heavier Fractions for the GPA Peng-Robinson Programs. Gas Processors Association.

Saryazdi, F., Motahhari, H., Schoeggl, F. F. et al. 2013. Density of Hydrocarbon Mixtures and Bitumen Diluted With Solvents and Dissolved Gases. *Energy Fuels* **27** (7): 3666–3678. https://doi.org/10.1021/ef400330j.

Svrcek, W. Y. and Mehrotra, A. K. 1982. Gas Solubility, Viscosity and Density Measurements for Athabasca Bitumen. *J Can Pet*

Technol **21** (4): 31–38. PETSOC-82-04-02. https://doi.org/10.2118/82-04-02.

Tavakkoli, M., Panuganti, S. R., Taghikhani, V. et al. 2013. Precipitated Asphaltene Amount at High-Pressure and High-Temperature Conditions. *Energy and Fuels* **28** (3): 1596–1610. https://doi.org/10.1021/ef401074e.

Venkatramani, A. and Okuno, R. 2016. Compositional Mechanisms in SAGD and ES-SAGD With Consideration of Water Solubility in Oil. Presented at the SPE Canada Heavy Oil Technical Conference, Calgary, 7–8 June. SPE-180737-MS. https://doi.org/10.2118/180737-MS.

Yazdani, A., Alvestad, J., Kjonsvik, D. et al. 2011. A Parametric Simulation Study for Solvent Co-injection Process in Bitumen Deposits. Presented at the Canadian Unconventional Resources Conference, Calgary, 15–17 November. SPE-148804-MS. https://doi.org/10.2118/148804-MS.

Zirrahi, M., Hassanzadeh, H., and Abedi, J. 2015a. Prediction of CO_2 Solubility in Bitumen Using the Cubic-Plus-Association Equation of State (CPA-EOS). *J. Supercritical Fluids* **98:** 44–49. https://doi.org/10.1016/j.supflu.2015.01.001.

Zirrahi, M., Hassanzadeh, H., and Abedi, J. 2015b. Prediction of Water Solubility in Petroleum Fractions and Heavy Crudes Using Cubic-Plus-Association Equation of State (CPA-EoS). *Fuel* **159:** 894–899. https://doi.org/10.1016/j.fuel.2015.07.058.

Zou, X. Y., Zhang, X., and Shaw, J. A. 2007. Phase Behavior of Athabasca Vacuum Bottoms + *n*-Alkane Mixtures. *SPE Prod & Oper* **22** (2): 265–272. SPE-97661-PA. https://doi.org/10.2118/97661-PA.

Zúñiga-Hinojosa, M. A., Justo-García, D. N., Aquino-Olivos, M. A. et al. 2014. Modeling of Asphaltene Precipitation From *n*-Alkane Diluted Heavy Oils and Bitumens Using the PC-SAFT Equation of State. *Fluid Phase Equilibr.* **376:** 210–224. https://doi.org/10.1016/j.fluid.2014.06.004.

Recommended Reading.

Li, H., Yang, D., and Li, X. 2012. Determination of Three-Phase Boundaries of Solvent (s) -CO_2 -Heavy Oil Systems Under Reservoir Conditions. *Energy Fuels* **27** (1): 145–153. https://doi.org/10.1021/ef301549a.

Appendix A—Measured PV Data for Bitumen at 140.2°C

Fig. A-1 shows the measured PV data for bitumen at a temperature of 140.2°C. Only single liquid phase and liquid/vapor phase equilibria were observed at this temperature. The saturation point is determined as the intersection of two PV curves.

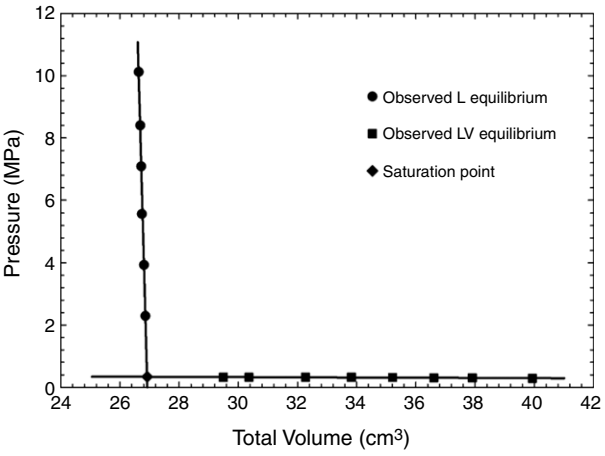

Fig. A-1—Measured PV data for bitumen at 140.2°C.

Appendix B—Measured PV Data for Mixture B at Different Temperatures

Fig. B-1 shows the measured PV data for Mixture B at temperatures ranging from 50 to 160.2°C. The L_1 phase is rich in bitumen, and the L_2 phase is rich in *n*-butane. Estimated phase boundaries were based mainly on visual observation. Each phase boundary was also confirmed by drawing two trend lines representing two types of phase equilibria, and locating the intersection of these two PV curves.

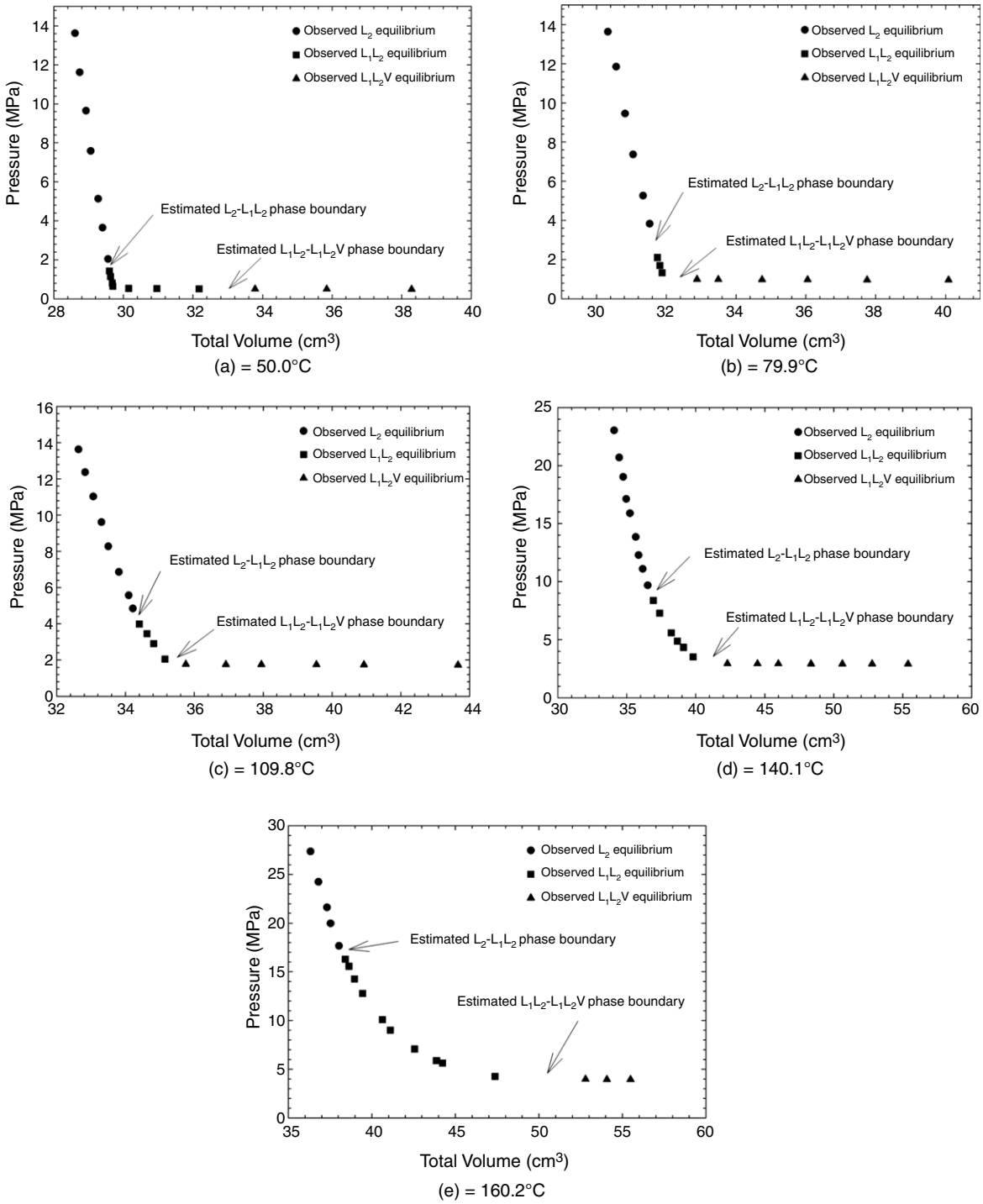

Fig. B-1—Measured PV data for Mixture B at different temperatures.

Appendix C—Measured PV Data for Mixture C at Different Temperatures

Fig. C-1 shows the measured PV data for Mixture C at temperatures ranging from 80 to 159.9°C. Estimated phase boundaries were based on visual observation and confirmed by plotting PV curves.

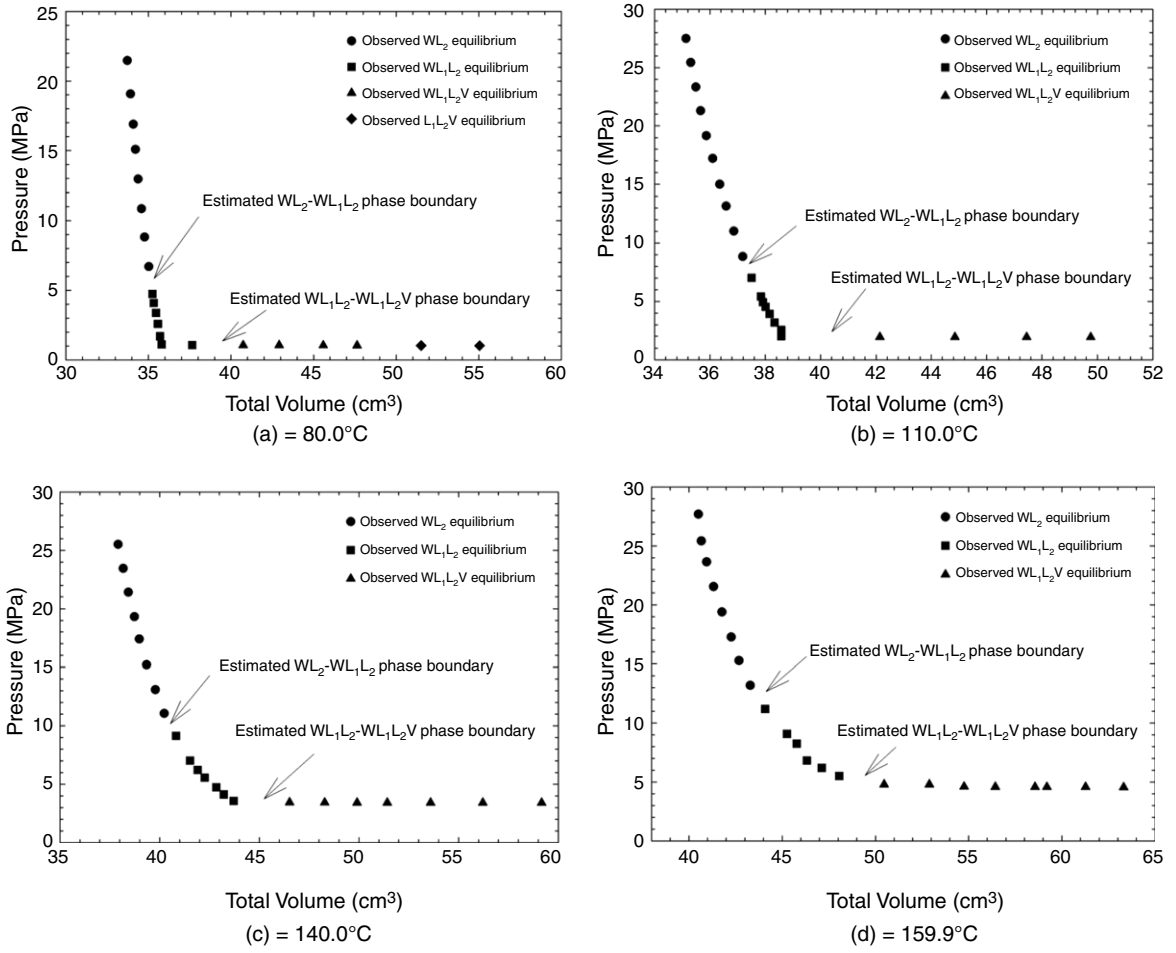

Fig. C-1—Measured PV data for Mixture C at different temperatures.

Jianyi Gao is an MSc degree candidate in petroleum engineering in the Department of Civil and Environmental Engineering at the University of Alberta. Her research interests include multiphase behavior, thermodynamics, and heavy-oil recovery. Gao holds a BS degree in petroleum engineering from the China University of Petroleum (Beijing). She is an SPE member.

Ryosuke Okuno is an assistant professor in the Department of Petroleum and Geosystems and Engineering at the University of Texas at Austin. Before his current position, he served as an assistant professor of petroleum engineering at the University of Alberta from 2010 to 2015. Okuno also has 7 years of industrial experience as a reservoir engineer with Japan Petroleum Exploration Company, and is a registered Professional Engineer in Alberta, Canada. His research and teaching interests include enhanced oil recovery (EOR), heavy-oil recovery, numerical reservoir simulation, thermodynamics, multiphase behavior, and applied mathematics. Okuno is a recipient of the 2012 SPE Petroleum Engineering Junior Faculty Research Initiation Award, is an associate editor for *SPE Journal* and *Journal of Natural Gas Science & Engineering (JNGSE)*, and holds the Pioneer Corporation Faculty Fellowship in Petroleum Engineering at the University of Texas at Austin. He holds BS and MS degrees in geosystem engineering from the University of Tokyo, and a PhD degree in petroleum engineering from the University of Texas at Austin.

Huazhou Andy Li is an assistant professor in petroleum engineering at the University of Alberta. His research interests include experimental and theoretical studies on the phase behavior of reservoir fluids, carbon dioxide (CO_2) EOR, surfactant-alternating-gas flooding, thermal and nonthermal heavy-oil recovery, stimulation of tight-oil/gas reservoirs with supercritical CO_2, and production optimization of oil reservoirs that is based on reservoir simulations. Li has authored or coauthored 26 peer-reviewed technical papers and has presented 16 papers at SPE and other international conferences. He holds a BSc degree and an MSc degree, both in petroleum engineering, from the China University of Petroleum (East China) and a PhD degree in petroleum-systems engineering from the University of Regina. Li began serving as an associate editor for *JNGSE* in 2014. In 2015, he received the Outstanding Contribution in Reviewing award from *JNGSE*. Li also serves as a technical reviewer for several academic journals, including *SPE Journal*. He is a member of SPE and the American Chemical Society.